Foundation University Journal of Engineering and Applied Sciences

FUJEAS
Vol. 4, Issue 1, 2023.
DOI:10.33897/fujeas.v4i1.789

Research Article

Article Citation:
Ijaz et al. (2023). "Glaucoma Detection using Fundus Images by Extracting Localized Disc Features". *Foundation University Journal of Engineering and Applied Sciences*
DOI:10.33897/fujeas.v4i1.789

Published by Foundation University Islamabad.
Web: https://fui.edu.pk/

Glaucoma Detection using Fundus Images by Extracting Localized Disc Features

Ayesha Ijaz, Zobia Suhail *

Department of Computer Science, Faculty of Computing and Information Technology, University of the Punjab, Lahore, Pakistan

***Corresponding Author:** zobia.suhail@pucit.edu.pk

Abstract:

Glaucoma is one of the leading causes of blindness worldwide. It occurs due to high pressure in the eyes and other factors such as family history, age, ethnicity, etc. It damages the optic nervous system which is irreversible damage. That's why regular screening for glaucoma is crucial and recommended. Researchers are continuously searching for better methods to identify glaucoma at early stages before it becomes worse and incurable. Significant work has been conducted on it, but there is still room for improvement. The main goal of this study is to propose a reliable system for glaucoma detection that considers the key factors contributing to glaucoma development, in accordance with the decisions made by clinical experts. In this work, the U-net model is used with EfficentNetb3 as a backbone model for optic disc and optical cup segmentation. In addition, a general deep learning model that has 1D convolution layers and other basic layers is used for glaucoma classification. Features extracted from optical disc and optical cup are used to train the deep learning model and overall 95% classification accuracy and 0.92 AUC are achieved for glaucoma classification on the RIGA dataset.

Keywords: Optic Disk and Optic Cup (OD and OC); Glaucoma; ROI; Retinal Fundus Images; Image Classification; CDR; Optic Nerve Head (ONH).

1. Introduction

Glaucoma, as per WHO data [2], ranks second in global blindness causes. In Pakistan, more than 1.8 million patients suffer from glaucoma, with nearly half experiencing permanent vision loss due to diagnostic and treatment delays [2].Glaucoma disproportionately affects Asians and women, standing as the second leading cause of blindness worldwide. By 2020, the number of individuals with OAG and ACG will reach 79.6 million, with 74% of them having OAG[1] .Although everybody can get glaucoma, some populations are more vulnerable. Glaucoma is 6–8 times more common in African Americans than in White people. Those who have diabetes are twice as likely to get glaucoma as those who do not. Glaucoma damages the visual nerve irreparably if it is left untreated, which results in blindness. Therefore, Early glaucoma diagnosis is crucial for managing the disease's primary medical therapy in an effective manner. The study of existing glaucoma detection methods and the formulation of a novel glaucoma detection strategy are the key objectives of this research. The difficulty during cup and disk segmentation may result from the use of additional filters and morphological processes to remove veins during pre-processing steps. Machine learning and deep learning approaches provide good accuracy for the detection of glaucoma as compared to image processing techniques [3]. Without using conventional image processing methods, the objective is to obtain more accuracy in comparison to other methodologies described in the literature.

2. Literature Review

While significant research has been conducted on improving glaucoma diagnosis, there is still a need for further advancement. In this section, we will assess current methods for detecting glaucoma and segmenting the OC(OC), along with their limitations.

Almazroa et al. developed glaucoma detection system using image processing techniques. They applied a localizing technique to get the ROI(ROI). Afterward, they performed manual segmentation marking and then calculated horizontal and vertical cup to disk ratio to determine the presence or absence of glaucoma [3]. Vishal Jindal in his work associated glaucoma with different body diseases that are also degenerative such as Alzheimer, osteoporosis, etc., [4]. Adnan Haider et al. suggested two networks in their work; the separable linked SLS-Net and the separable linked SLSR-Net, to solve the issue that the OC boundaries are not very clear that makes it difficult to accurately segment the OC and accurately segment the OC and OD at the pixel level [5]. An automated glaucoma diagnosis technique was developed by H. N. Veena et al. [7] where they performed some preprocessing before giving the images as input to both CNN models that are used for optic disc and cup segmentation. After segmentation, they calculate cup to disk ratio for glaucoma detection. Yuji Hatanaka et al., explain a better method that makes use of the blood vessel bends that help them to improve their accuracy in glaucoma detection method [7]. Arunava Chakravarty et al., In their study, proposed a Multi-task Convolutional Neural Network (CNN) that simultaneously separates the OC(OC) in color fundus pictures and detects the occurrence of glaucoma [8]. Rongchang Zhao et al., present a unique WSMTL strategy for precise evidence recognition, optic disc segmentation, and automated glaucoma detection [9]. Chisako Muramatsu et al. proposed a technique for detecting retinal nerve fiber layer defect which is also the symptom of glaucoma [10]. Jose Ignacio Orlando et al. performed an analysis using a CNN model for glaucoma detection that was pre-trained on non-medical data [11].

Welfer et al. [13] propose an adaptive method for ODsegmentation based on mathematical morphology and vascular structure modeling. This method includes two stages: first, detecting the OD location by analyzing the main vessels arcade, and second, delineating the OD boundary using the watershed transform. Shubnam Joshi et al. [14] used datasets from different sources that were then passed as input to pre-trained CNN models Resnet, VGGNET-16, and GoogLeNet. Subsequently, the output of these models is combined in a prediction vector and then the decision is finalized based on majority voting that either the images are normal or glaucoma-affected. V. Elizabeth Jesi et al., proposed a machine learning model for glaucoma classification. HSV features are used to enhance the image and blood vessels are removed from images. Subsequently, a K-mean optimization method is applied for better accuracy of glaucoma classification [14]. Cheng and Huang used an adaptive thresholding technique to localize and segment the optic disc (OD). They determined the threshold (T) based on the brightest spot in the fundus image and chose the red channel due to its minimal blood vessels as distractions. The object with the most 8-connected pixels was selected. By using a deep learning approach Syna Sreng et al., proposed their two-stage deep learning model for the detection of glaucoma. In the first stage their DeepLabv3+ model segments the optic disc by semantic segmentation and then in the second stage classification of normal and glaucoma-affected images is done [16].

Munazza Tabassum et al. proposed a model named CDED-Net for the joint segmentation of OC for glaucoma detection in which they used eight different convolution layers in encoder and decoder block, whereas at encoder stage re-use of feature technique is used to improve the accuracy and network's efficiency [17]. Muthu Rama Krishnan M et al. proposed an inexpensive automated glaucoma diagnosis system that draws hybrid features from digital fundus images [18]. Qaisar Abbas in his research, proposed a system referred as Glaucoma-Deep. In this model, features were extracted from raw image intensities using a multi-layer CNN architecture that was unsupervised [19]. Hafsah Ahmad et al. proposed a glaucoma detection technique where characteristics from retinal fundus images are extracted and used to classify glaucoma by computing CDR. Another feature for glaucoma detection is the Ratio of Neuroretinal Rim in the inferior, superior, temporal, and nasal quadrants, or "ISNT quadrants" which is also computed in their work for glaucoma detection. They implemented their method

on 80 retinal images [20]. Atalie C. Thompson et al., proposed a Deep Learning (DL) algorithm that assesses the glaucoma damage from SD-OCT B scan images that did not have segmentation lines [21]. WangMin Liao et al., proposed a unique clinically interpretable Con-Net design called EAMNet (evidence activation mapping) for more transparent interpretation by emphasizing the different regions that the network recognizes, in addition to providing an accurate glaucoma diagnosis [22]. In [24], deep neural networks were employed for optic disc segmentation. The authors utilized faster R-CNN, extracting various features from the dataset images [24]. Afolabi O. Joshua et al. employed an improved U-net CNN model for segmenting the optic cup and disc [25]. Fauzia Khan et al. introduced an image processing technique for early glaucoma detection. They classify glaucoma by extracting two features from retinal fundus images: (i) CDR and (ii) Ratio of Neuroretinal Rim in inferior, superior, temporal, and nasal quadrants [26]. Muthu Rama Krishnan Mookiah et al. proposed an innovative method of optic disc segmentation using intuitionistic fuzzy histon [27]. Zhuo et al. [28] presented a multimodality fusion approach to detect the optic cup. They evaluated various segmentation and boundary detection methods to enhance neuro-retinal optic cup estimation accuracy. Muhammad Naseer Bajwa et al. proposed a two-stage deep learning classification model for glaucoma detection. The first stage locates and extracts the optic disc using RCNN, while the second step categorizes the extracted disc as healthy or glaucoma-affected using Deep CNN [29]. In [3], an adaptive local thresholding technique generates a binary image. Large connected components representing major vessels are extracted from this image. The remaining fragments, including thin vessel segments or pixels, are then classified using SVM.

3. Material

For this work, two datasets are used that are publicly available. One dataset for retinal vessel segmentation and other datasets for OD and OC segmentation and glaucoma classification. The first dataset is retrieved from Kaggle (https://www.kaggle.com/code/ipythonx/retinal-vessel-segmentation-starter/input) which is primarily used for vessel segmentation. There are four folders in this dataset but we used only the DRIVE folder for this work. The test and train folder contains 20 images with their associated masks. All images of this dataset have dimensions 565 x 584p and are saved in tiff and gif format. The second dataset is RIGA- the Retinal Fundus Images for Glaucoma Analysis is a published and licensed dataset [2] that is used for OD and OC segmentation and also for glaucoma classification. This dataset consists of three folders: Folder Messidor consists of 460 images. The size of the images in this folder are 2240 x 1488p and 1440 x 960p. Folder Magrabia contains 95 images of which 48 images are of females and 47 images are of males. The size of the images in this folder is 2743 x 1936p. Folder Bin rushed contains 195 images. The size of the images in this folder is 2376 x 1584p. The entire RIGA dataset contains 750 images that are used as original images and 4500 images that are ground truth images of the original images. All the Dataset images are saved in tiff and jpg format. This dataset has no separated folders for normal and glaucoma-affected images. For automated glaucoma detection, there is a need for ground truth regarding glaucoma-affected or normal images. Therefore, the RIGA dataset is partially marked for the ground truth from an expert eye specialist doctor as normal, glaucoma, and suspected. From the 750 total images (taken for experiments), there are 54 glaucomatous images and 71 suspected images, and the remaining are considered as normal images.

4. Proposed Method

The approach employed in this study involves several steps. Initially, retinal fundus images undergo pre-processing steps such as resizing, normalization, and data augmentation. Following this, a deep learning model is used for OC(OC) segmentation. Once the disk segmentation is done, the ROI is extracted. Subsequently, using the same deep learning model, retinal vessel segmentation is performed, and another ROI is obtained comprised of boundary around the Optical Disc region after removing the vessels. Finally, texture-based features of the cup and disk are computed separately and fed into our proposed deep-learning model for classification. The proposed methodology is shown in Figure 1.

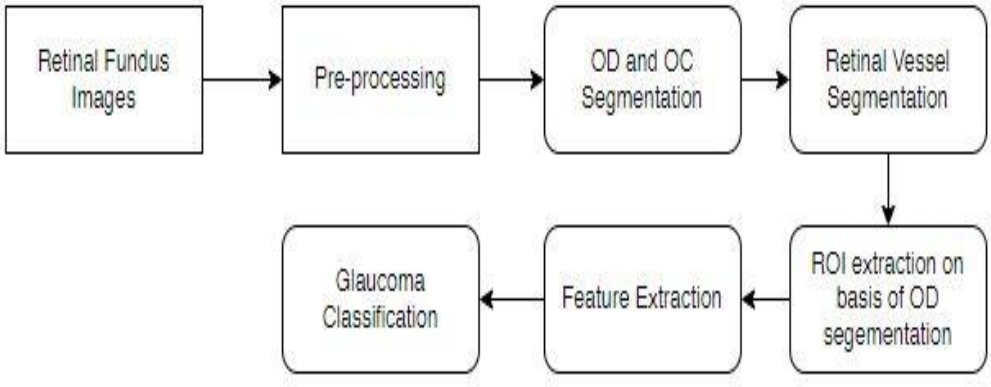

Figure 1: Methodology flow

4.1. Pre-processing

In pre-processing, first, the image is resized with dimensions 224 x 224 because the original dimensions of the images were too large for giving them as input to subsequent steps. Subsequently, Normalization is performed normalization on the resized images and the range is set between 0 and 1 of pixel values by dividing each pixel of the image by 255. It guarantees that each input (in this case, each pixel value) is drawn from a standard range.

4.2. Data Labelling

Machine and deep learning models can be trained using provided masks to label entire images or recognize specific groups of items within an image. While the RIGA dataset contains images along with their ground truth, the ground truth for the OC are not available in a format suitable for training deep learning models. To train our deep learning segmentation model effectively, it is essential to have labels for the cup and disk. Therefore, we labeled the masks for OC and OD using LabelMe software.

4.3. Data Augmentation

In this work, we used the widely used technique of Data Augmentation in machine learning and computer vision. Data augmentation aims to increase the training dataset's size by generating modified versions of existing data samples. This technique is crucial for preventing overfitting during model training. Various transformations are employed to create diverse data samples, such as rotations, flips, scaling, and color adjustments. Additionally, data augmentation enhances the model's ability to extract features. In our study, we specifically apply random horizontal flips, rotations up to 45 degrees, and slight variations in brightness and contrast.

4.4. Segmentation Model Architecture

For segmentation, we used a modified U-net model with EfficentNetb3 as a backbone model for the segmentation of OC and OD regions as well as for vessel segmentation. The EfficentNetb3 model is used as the encoder part and the U-net model is used as the decoder part in our proposed segmentation model. The details of both model architecture and their benefits are described in the following subsections.

4.4.1. U-net Model

A popular deep-learning model for semantic segmentation is called U-Net. In jobs like biomedical image segmentation, where accurate delineation of structures becomes vital, U-Net has been very successful

U-Net uses both an ”expansive” and a ”contracting” approach to build its extensive features. Figure 2 shows our modified segmentation model. In our proposed model in decoder side U-net layers are implemented. The decoder is the U-Net architecture's second element. The low-resolution image feature maps are upsampled to the encoder's original input image size. With concatenation operations and a number of upsampling layers, the decoder combines the matching feature maps from the encoder. The feature maps' spatial dimensions are increased by the upsampling layers while maintaining their channel-wise data. The last Upsampling layer in our model upsampled the previous layer's 112 x112 dimension to 224 x 224 dimension which is the same as our input image dimension. The concatenated feature maps help in the recovery of fine-grained details by integrating high-resolution data from the encoder. Figure 2 shows the concatenation like from the encoder side Block6a concatenate with decoderblock0. In each decoder block as shown in Figure 3 we have 2 Convolution blocks whose objective is to extract features from its input data. Activation, batch normalization, and convolutional layers are utilized in succession. A deep learning model's non-linearity and solving the problem of vanishing gradients are introduced by the rectified linear unit (ReLU), an activation function. In the output block of our modified U-net model, we have 2 conv blocks, Upsampling and additional convolution layer and a softmax layer. In the output block, the last two extra layers are added for better processing of output and introducing more non-linearity in the model [30].

4.4.2. EfficentNetb3 Model

EfficientNet is one of the more significant Convolution Neural Networks among a large number of them. Compared with all of its predecessors, it has provided improved performance. In CNN designs, scaling up (raising the number of layers) is typically a laborious process because there are many different ways to scale up. Manual selection of the perfect combination takes a lot of time. EfficientNet uses a new scaling technique that uses a straightforward but incredibly effective compound coefficient to equally scale all depth, width, and resolution parameters for better results. All models from B1 to B7 have the same base layers but as the model becomes updated the number of layers is increased as EfficentNetb0 has 237 layers and B7 has 813 layers. It is clear that the architecture uses seven inverted residual blocks, although they all have unique configurations. SE blocks are also used in these blocks. Like Block 1 has 1a and 1b and both of them have multiple layers that perform multiple functions. Block 1a contains Depthwise convolution, batch normalization, activation, global average pooling layer for squeeze purpose, excitation block, and reshape layer (part of SE block). Many of these layers are also repeated in this block like convolution, activation, and batch normalization. Each block of Efficentnetb3 as shown in Figure 2 further consists of multiple blocks that have many layers as we described in block1a. Block2 has (2a,2b,2c), Block3 has (3a,3b,3c), Block4 has (4a,4b,4c,4d,4e), Block5 has (5a,5b,5c,5d,5e), Block6 has (6a,6b,6c,6d,6e,6f), and Block7 has (7a,7b). EfficentNetb3 uses depth-wise convolution, contrary to normal CNNs, where convolution is performed to all M channels at once, the depth-wise operation only applies convolution to one channel at a time [30].

4.5. Extract Region of Interest

After OD and OC segmentation, ROI is extracted on the basis of OD segmentation as shown in Figure 4. Afterward, canny edge detection is applied on the predicted mask of the segmentation model for getting the edges of the disk mask. After getting the edges of the optic disk, minimum x and y also maximum x and y surrounding the optical disk are retrieved to get refined ROI. Following this, the size of the ROI is increased by 10 percent in both width and height. The enlarged ROI dimensions are then used for obtaining the ROI after vein segmentation.

4.6. Retinal Vessel Segmentation and Vessel Removal from OD and OC ROI

For glaucoma classification, features are extracted features from the OD and OC regions. To enhance feature extraction from these regions, retinal vessel segmentation is performed to remove vessel areas from the OD and OC regions. Vessel segmentation aids in extracting only the pertinent features from the OD and OC regions, excluding vessel areas, for more accurate glaucoma classification. The same

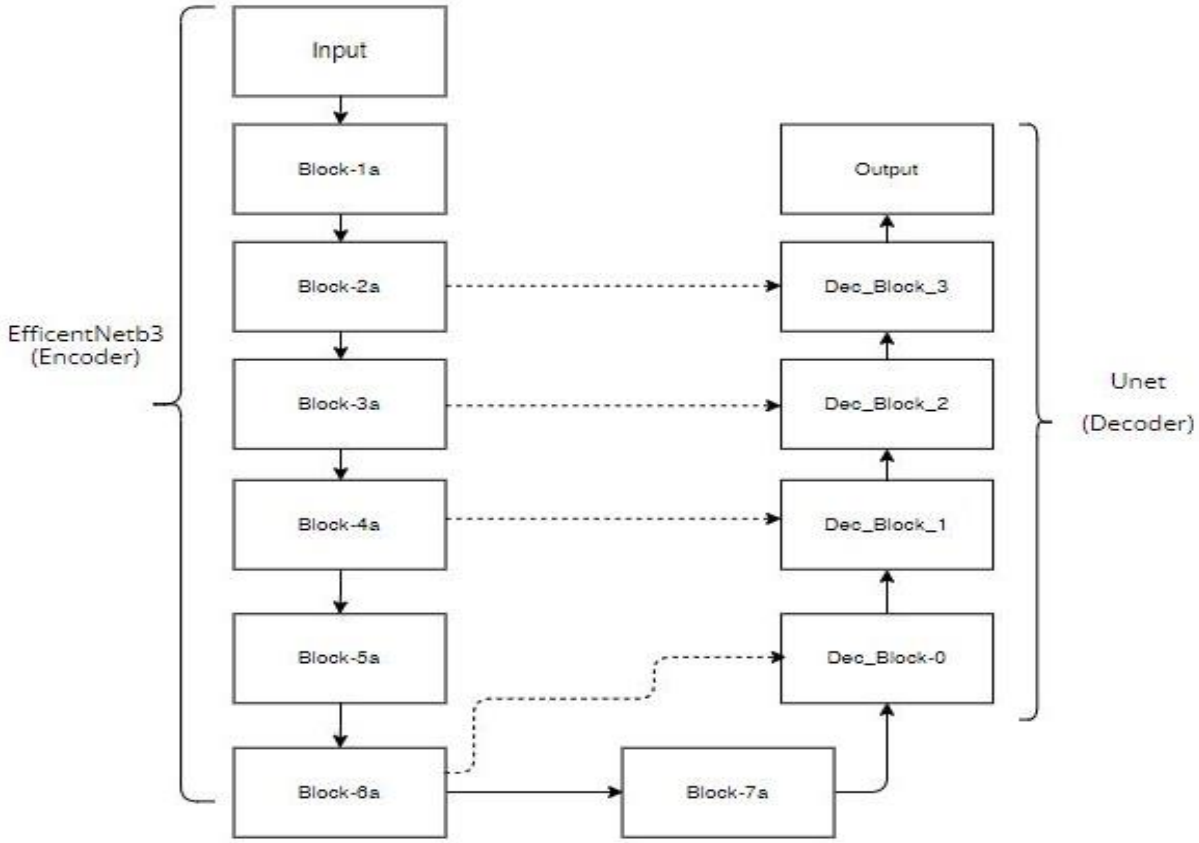

Figure 2: Proposed segmentation model

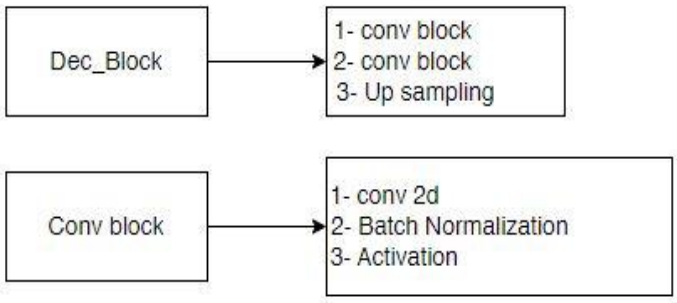

Figure 3: Dec and Convolution block detail

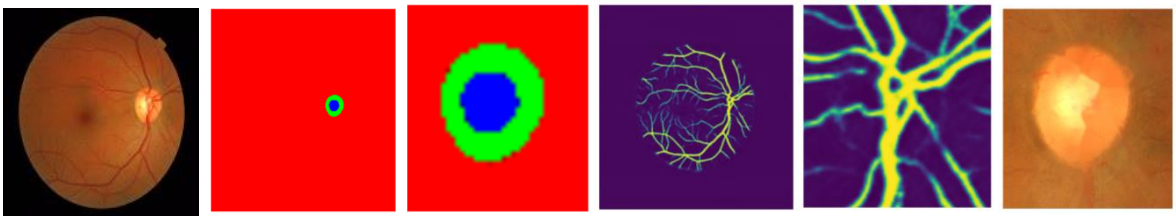

(a) (b) (c) (d) (e) (f)

Figure 4: ROIand Vessel removal results. (a) original image, (b) segmentation model output, (c) ROI of predicted output, (d) vein segmentation model output, (e) ROIof predicted output, (f) vein removal and ROIfrom the original image

segmentation model used for OD and OC segmentation was employed for vessel segmentation (Section 4.4). The results of vessel segmentation on a sample image from the dataset are depicted in Figure 4(d).

After vessel segmentation, a ROI of the same size as for OD and OC regions is extracted from the segmented vessel image to remove vessels from those regions (Figure 4(e)). The vein region was extracted so that the vein area could be filled by the surrounding pixel values, effectively removing vessels from the OD and OC area (Figure 4(f)).

4.7. Feature Extraction

Texture features are extracted from OD and OC ROIs using GLCM-based features. Features are computed on both separable images of OD and OC. To get deep details of the texture, first, the image is divided into patches (on average 158 patches per image) for OD and OC regions. Afterward, texture features are computed that include dissimilarity, correlation, entropy, mean, variance, median, skewness, and kurtosis of each patch. The formulas to compute these texture features are shown below:

$$\text{Dissimilarity} = \sum_{a,b=0}^{M-1} X_{a,b} \ |a-b| \tag{1}$$

$$\text{Correlation} = \sum_{a,b=0}^{M-1} X_{a,b} \ \frac{(a-\mu_a)(a-\mu_b)}{\sqrt{(\sigma_a)^2 (\sigma_b)^2}} \tag{2}$$

$$\text{Entropy} = \sum_{a,b=0}^{M-1} X_{a,b} \ (-\ln X_{a,b}) \tag{3}$$

$$\text{Mean} = \mu_a = \sum_{a,b=0}^{M-1} aX_{a,b}\,, \mu_b = \sum_{a,b=0}^{M-1} bX_{a,b}\,, \mu = \frac{\mu_a+\mu_b}{2} \tag{4}$$

$$\text{Variance} = \sigma_a^2 = \sum_{a,b=0}^{M-1} X_{a,b}(a-\mu_a)^2\,, \sigma_b^2 = \sum_{a,b=0}^{M-1} X_{a,b}(b-\mu_b)^2\,, \sigma^2 = \frac{\sigma_a+\sigma_b}{2} \tag{5}$$

$$\text{Skewness} = \frac{\sum_{i=1}^{N}(q_i-\bar{q})^3}{\sigma^3} \tag{6}$$

$$\text{Kurtosis} = \frac{\sum_{i=1}^{N}(q_i-\bar{q})^4}{\sigma^4} \tag{7}$$

Here, $X_{a,b}$ = the probability that values a and b will appear in neighboring pixels in the original image within the window defining the neighborhood, a = the columns, and b = the rows.

The median is determined after numerically ordering all of the values of the pixels from the window and choosing the middle pixel value. In Figure 5 cup and disk areas are shown with vessel removal that are further for feature extraction. It's crucial to note that features are computed separately for both the OD and OC regions, treating them as distinct entities with varying contributions to glaucoma appearance.

4.8. Classification Model Architecture

For classification, a general deep learning model is proposed as shown in Figure 6 that has basic layers

(a) (b) (c)

Figure 5: (a) optic cup and disk segmentation result, (b) extracted cup area, (c) extracted disk area

and is easy to understand. This model has three 1D convolution layers along with max-pooling and activation layers and 2 dense layers at the end. Text and 1D signals are the two main applications of 1D Convolution. The kernel flows in a single direction, from right to left (for feature values). The values on the feature map display the position and importance of each feature. In the activation layer sigmoid activation function is used. The sigmoid function is useful in data analytics and many other domains since it can convert any real number to a value between 0 and 1. It contributes to the classification model by providing non-linearity, transforming outputs into probabilities, facilitating probabilistic interpretation of predictions, and defining a clear decision boundary between classes. To input data from a 1-D array into a classification model, we employ a technique called flattening, which transforms multidimensional arrays into 1-D arrays. The Dropout layer helps prevent overfitting in models. During each training update, the outgoing edges of hidden units (neurons in hidden layers) are randomly set to 0, as part of Dropout. Neurons in the simple layer (also known as the fully connected layer) receive information from every cell in the layer below. Based on the results from convolutional layers, a dense layer is used for image categorization. Using the classification model trained on features computed from cup and disk patches (as shown in Figure 6), images are classified as normal or glaucoma images. The model's output represents results in 0-1 form, where 0 corresponds to normal and 1 to glaucoma.

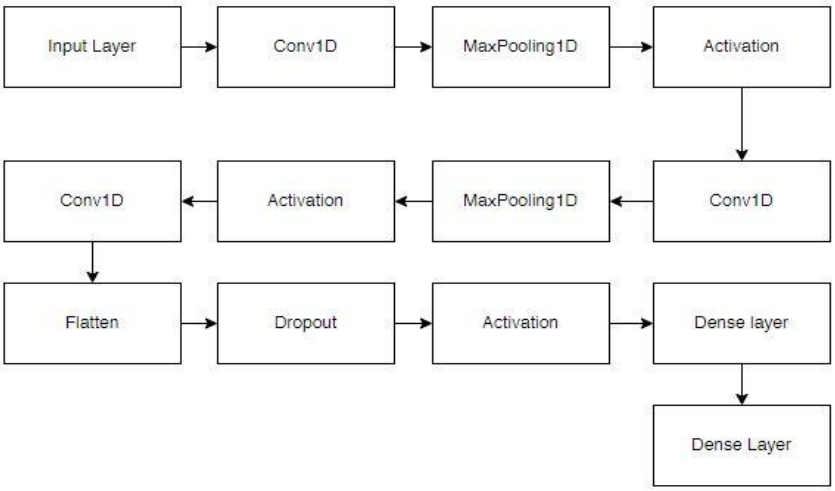

Figure 6: Proposed classification model

5. Experimentation

The model takes in an image with dimensions of 224 x 224 as input. It's vital to remember that these measurements constitute a color channel image, with each pixel denoting the image's brightness or intensity level. The encoder section gathers feature representations while downsampling the input image.

Many depth-wise convolutional layers are applied to get deep feature extraction from the image. The convolution layer along with batch normalization and activation layers are also implemented. All 7 blocks that are shown in Figure 2 on the encoder side are used for the enhancement of the capability of the feature extraction. In order to decrease the spatial dimensions and avoid overfitting, dropout techniques are used. Block 7 acts as a bridge between the encoder and decoder section as shown in Figure 2. Skip connection is also used for some Blocks of the encoder side. Block2a, 3a, 4a, and 6a are used as a skip connection and concatenate with decoder block 3,2,1,0 respectively. The decoder side makes it possible to locate objects precisely. The feature maps are upsampled and the desired output is rebuilt in the decoder portion. The layers detail of the decoder side is also shown in Figure 5. From the output layer of the encoder side, we get the predicted mask.

The computer specifications used for implementation include an i7 CPU, 16 GB RAM, and a Nvidia GeForce GTX 1060 with 6 GB GPU. Overall work was conducted on the Google Colab platform. TensorFlow was employed to implement the suggested model, with TensorFlow version 2.12 and Python version 3.10 present in the software environment. Adam optimizer is used with a learning rate

of 1e-4 to train the models. The dice coefficient loss function, suitable for segmentation tasks, was utilized. During training, the dataset was iterated over with a batch size of 4 for segmentation tasks and 16 for classification tasks. After several trials to determine an appropriate number, 100 epochs were chosen for training the segmentation model, and 200 epochs for the classification model to achieve minimal loss. It has been discovered that training for more epochs might result in overfitting, in which the model becomes overly specialized to the training data and operates badly on new, untainted data. For the segmentation model for OD and OC area, 80% of the data from the RIGA dataset is used for training, while the remaining 20% is used for testing. Data augmentation is also used in this approach so the model can also give a good result on unseen data in the future. The segmentation model is trained on the labeled data that is already marked using Labelme software on the basis of ground truth. 70:30 train-test split ratio is used for the classification model, where the model is trained on eight texture features that are computed from cup and disk patches separately.

5.1 Performance Evaluation Parameters

For performance evaluation metrics, Dice Coefficient (DSC) and Intersection over Union (IOU) are utilized to assess the segmentation model's performance. For the classification model, Accuracy, F1 score, Precision, and Recall are used as classification performance evaluation metrics. Predicted segmentation masks and the ground truth mask are denoted as A and B, respectively. The total number of pixels within each set is indicated by |A| and |B|. The intersection of the two sets is denoted by the expression |A ∩ B|, representing the shared pixels between the two sets.

$$\text{Dice Coefficient} = \frac{2 * |A \cap B|}{|A| + |B|} \tag{8}$$

$$\text{Dice Loss} = 1 - \text{Dice Coefficient} \tag{9}$$

$$\text{IOU} = \frac{|A \cap B|}{|A \cup B|} \tag{10}$$

$$\text{Accuracy} = \frac{TN + TP}{TN+TP+FN+FP} \tag{11}$$

6. Results and Discussions

This RIGA dataset was only used by some researchers for OD and OC segmentation but no one utilized this dataset for classification because there is no ground truth marked as a normal or glaucoma label. For this work, the RIGA dataset is marked for Normal, Glaucoma, or suspicious cases by the eye specialist doctor. Some images in this dataset show the early stages of glaucoma where the cup size is not significantly increased. Consequently, the CDR may not be an effective factor for characterizing such cases as glaucoma. In contrast, the proposed method of extracting texture features from the disk and cup areas is more helpful in classifying images as glaucomatous rather than relying solely on CDR. Figure 7 shows the segmentation results for some of the sample images from the dataset. The proposed segmentation model gives IOU 0.856, Dice loss 0.247, and Dice Coefficient 0.75. Whereas, 95% accuracy, 0.90 f1 scores, 0.89 precision, and 0.90 recall are achieved for the proposed classification model.

Figure 8 and Figure 9 present additional segmentation results from the dataset. In Figure 8, refined segmentation boundaries are evident, while Figure 9 displays some boundaries that are ill-defined. However, these ill-defined do not affect the overall classification results. Patients with glaucoma experience changes in their eye structure, which is why we opted for texture features for glaucoma classification. In our scenario, if the segmentation slightly deviates from the boundary marked by ophthalmologists, it's not a cause for concern because patients with glaucoma exhibit changes in their outer disk boundary. The feature from the outer boundary region is also valuable for glaucoma detection. Table 1 presents some glaucoma classification results compared with the ground truth. Upon analyzing the table, our model's predicted output is encouraging, but there are some inaccuracies in certain images, indicating that our model still requires improvement through further training on additional features.

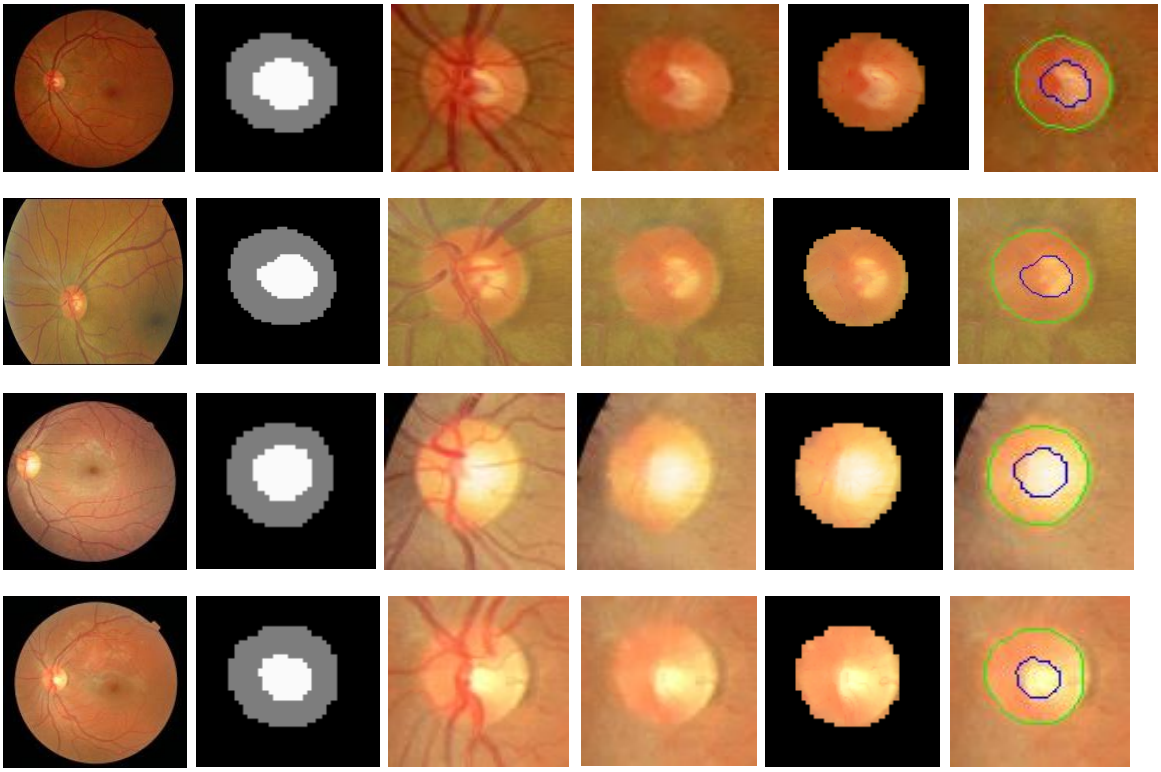

(a) (b) (c) (d) (e) (f)

Figure 7: output visualization, (a) original images, (b) ROIof predicted output, (c) ROIextracted from original image as per the calculated dimensions from (b), (d) vein removal from region of interest, (e) cup and disk areas from region of interest, (f) cup and disk segmented boundary blue line show cup boundary and green line show disk boundary

As explained in Section 3, the RIGA dataset is categorized by doctors into normal, glaucoma, and suspected cases. Suspected cases are further divided into suspected normal and suspected glaucoma, indicating a higher likelihood of developing glaucoma or remaining normal. In Table 2, the results of suspected cases are predicted by our classification model (as suspected normal or suspected by

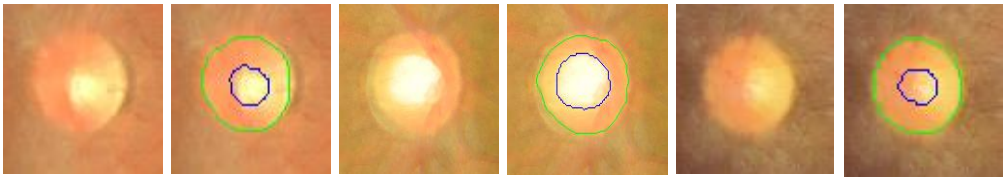

(a) (b) (c) (d) (e) (f)

Figure 8: Segmentation results with refined boundaries. (a),(c),(e) images are ROIimages whose segmentation is shown in (b),(d),(f).

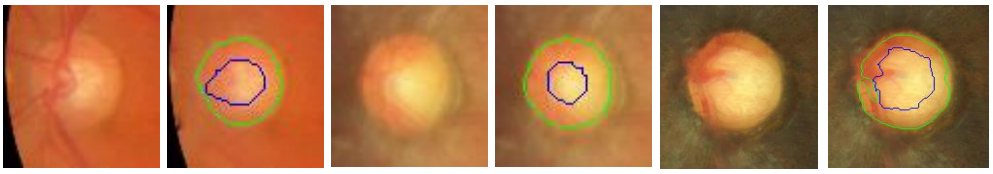

(a) (b) (c) (d) (e) (f)

Figure 9: Segmentation results with ill-defined boundaries. (a),(c), and (e) are ROIimages whose segmentation results are shown in (b),(d),(f).

Table 1: Glaucoma classification results

Image name	Folder name	Model Prediction	Ground Truth
Image9prime	Bin1	Glaucoma	Glaucoma
Image16prime	Bin4	Glaucoma	Glaucoma
Image33prime	Bin2	Glaucoma	Normal
Image35prime	Female	Normal	Normal
Image121prime	Messidor	Glaucoma	Normal

Table 2: Suspected glaucoma classification results

Image name	Folder name	Model Prediction	Ground Truth
Image31prime	Bin1	Glaucoma	Normal
Image17prime	Bin2	Normal	Glaucoma
Image34prime	Bin3	Normal	Normal
Image49prime	Bin4	Glaucoma	Glaucoma
Image160prime	Messidor	Normal	Normal

glaucoma), and then compared with the ground truth of suspected cases marked by eye specialist doctors.

The RIGA dataset mostly comprises cases in the early stages of glaucoma, but there is still a chance that these patients may be normal. This is confirmed by conducting additional tests on the patients to check their eye pressure and eye structure. In these instances, our model requires some improvement to detect the very early stages of glaucoma by training on multiple features.

6.1 Comparison with Existing Techniques

The comparison in Table 3 is based on the accuracy of the proposed models. Here, we evaluate several existing methods for classifying glaucoma and compare their effectiveness with our proposed approach. Adnan Haider et al. [6] utilized the Rim-One-r3 and REFUGE datasets. They performed OD and OC segmentation using deep learning methods, achieving good results, but relied on the Cup-to-Disc Ratio (CDR) parameter for glaucoma classification, with accuracies of 0.90 and 0.925. Shubham et al. [14] utilized the DRISHTI-GS, DRIONS-DB, HRF, PSGIMSR, and combined datasets. They employed an ensemble-based deep learning model for classification, achieving accuracies of 95%, 95%, 98%, 91%, and 88% respectively. V. Elizabeth Jesi et al. [15] used a private dataset and achieved 96% accuracy in glaucoma classification based on the CDR parameter, although they did not test on publicly available

Table 3: Glaucoma classification performance comparison

Author	Year	Dataset	Accuracy
Shubham [14]	2022	Four publicly available dataset	91%, 95%, 98%, 95%

Syna Sreng [17]	2020	Five publicly available dataset	97.37%, 90.0%, 86.84% and 99.53%
Adnan Haider [6]	2022	Two Publicly available dataset	0.90%, 0.92%
V.Elizabeth [15]	2021	private dataset	96%
Fan Guo [32]	2020	ORIGA dataset	0.84 %
Rahul Krishnan [33]	2020	Dristhi-GS	86%
Proposed method	2023	RIGA	95%

datasets. Syna Sreng et al. [17] utilized a two-stage system for glaucoma classification, achieving accuracies of 95% on REFUGE, 97% on RIM-ONE, 99% on ACRIMA, 86% on DRISHTI-GS1, and 90% on ORIGA datasets, with corresponding Area Under the Curve (AUC) values of 95%, 100%, 99%, 91%, and 92% respectively. From the comparison, it is important to note that the dataset used in this study has not been previously used for classification.

7. Conclusion and Future Work

In this study, we proposed a deep learning-based automated system for glaucoma classification, as well as OD and OC segmentation. Our proposed methodology achieved an accuracy of 95%, an F1 score of 0.90, precision of 0.89, and recall of 0.90 for glaucoma classification when compared against the ground truth. Our model also performed well on suspected patients. Although the results of our proposed approach for glaucoma classification are promising, there is still room for improvement to avoid false predictions. Therefore, our future focus will be on enhancing this method by testing it on larger datasets.

Acknowledgment

We would like to acknowledge Dr. Arslan Ashraf, an eye specialist at Hussain Memorial Hospital in Lahore, Pakistan, for his valuable time spent in marking the ground truth for the RIGA dataset, including normal, glaucomatous, and suspicious cases. We also thank him for providing insights on suspicious cases and distinguishing between suspicious normal and suspicious glaucoma cases.

8. References

[1] L. Khan, M. Ali, M. Qasim, F. Jabeen and B. Hussain, "Molecular basis of glaucoma and its therapeutical analysis in Pakistan: an overview," *Biomedical Research and Therapy*, vol. 4(03), pp.1210-1227, 2017.

[2] H. A. Quigley and A. T. Broman, "The number of people with glaucoma worldwide in 2010 and 2020," *British Journal of Ophthalmology*, vol. 90(3), pp. 262–267, 2006.

[3] H. N. Veena, A. Muruganandham and T. S. Kumaran, "A Review on the optic disc and optic cup segmentation and classification approaches over retinal fundus images for detection of glaucoma," *SN Applied Sciences*, vol. 2, pp. 1–15, 2020.

[4] A. Almazroa, S. Alodhayb, E. Osman, E. Ramadan, M. Hummadi, M. Dlaim, M. Alkatee, K. Raahemifar and V. Lakshminarayanan, "Retinal fundus images for glaucoma analysis: the RIGA dataset," In *Medical Imaging 2018: Imaging Informatics for Healthcare, Research, and Applications*, SPIE, 2018, vol. 10579, pp. 55–62.

[5] V. Jindal, "Glaucoma A multifactorial disease and its multidimensional management," *International Journal of Scientific and Research Publications*, vol. 3(3), pp. 21–23, 2013.

[6] A. Haider, M. Arsalan, M. B. Lee, M. Owais, T. Mahmood, H. Sultan and K. R. Park, "Artificial Intelligence-based computer-aided diagnosis of glaucoma using retinal fundus images," *Expert Systems with Applications*, vol. 207(C), 117968, 2022.

[7] H. N. Veena, A. Muruganandham and T.S. Kumaran, "A novel optic disc and optic cup segmentation technique to diagnose glaucoma using deep learning convolutional neural network over retinal fundus images," *Journal of King Saud University-Computer and Information Sciences*, vol. 34(8), pp. 6187–6198, 2022.

[8] Y. Hatanaka, Y. Nagahata, C. Muramatsu, S. Okumura, K. Ogohara, A. Sawada, K. Ishida, T. Yamamoto and H. Fujita, "Improved automated optic cup segmentation based on detection of blood vessel bends in retinal fundus images," In *Proceedings of 36th Annual International Conference of the IEEE Engineering in Medicine and Biology Society*, IEEE, 2014, pp. 126–129.

[9] A. Chakravarty and J. Sivswamy, "A deep learning based joint segmentation and classification framework for glaucoma assesment in retinal color fundus images," *arXiv preprint arXiv:1808.01355,* 2018.

[10] R. Zhao, W. Liao, B. Zou, Z. Chen and S. Li, "Weakly-supervised simultaneous evidence identification and segmentation for automated glaucoma diagnosis," *Proceedings of the AAAI Conference on Artificial Intelligence*, vol. 33(1), pp. 809–816, 2019.

[11] C. Muramatsu, Y. Hayashi, A. Sawada, Y. Hatanaka, T. Hara, T. Yamamoto and H. Fujita, "Detection of retinal nerve fiber layer defects on retinal fundus images for early diagnosis of glaucoma," *Journal of Biomedical Optics*, vol. 15(1), pp. 016021–016021, 2010.

[12] J. I. Orlando, E. Prokofyeva, M. del Fresno and M. B. Blaschko, "Convolutional neural network transfer for automated glaucoma identification," In *12th International Symposium on Medical Information Processing and Analysis*, SPIE 2017, vol. 10160, pp. 241–250.

[13] A. Almazroa, R. Burman, K. Raahemifar and V. Lakshminarayanan, "Optic disc and optic cup segmentation methodologies for glaucoma image detection: a survey," *Journal of Ophthalmology*, Article ID 180972, pp. 1–28, 2015.

[14] S. Joshi, B. Partibane, W. A. Hatamleh, H. Tarazi, C. S. Yadav and D. Krah, "Glaucoma detection using image processing and supervised learning for classification," *Journal of Healthcare Engineering*, Article ID 2988262, pp. 1–12, 2022.

[15] V. Elizabeth Jesi, S. Mohamed Aslam, G. Ramkumar, A. Sabarivani, A. K. Gnanasekar and P. Thomas, "Energetic glaucoma segmentation and classification strategies using depth optimized machine learning strategies," *Contrast Media & Molecular Imaging*, Article ID 5709257, pp. 1–11, 2021.

[16] V. S. Mary, E. B. Rajsingh and G. R. Naik, "Retinal fundus image analysis for diagnosis of glaucoma: a comprehensive survey," *IEEE Access*, vol. 4, pp. 4327–4354, 2016.

[17] S. Sreng, N. Maneerat, K. Hamamoto and K. Y. Win, "Deep learning for optic disc segmentation and glaucoma diagnosis on retinal images," *Applied Sciences*, vol. 10(14), pp. 1–19, 2020.

[18] M. Tabassum, T. M. Khan, M. Arsalan, S. S. Naqvi, M. Ahmed, H. A. Madni and J. Mirza, "CDED-Net: Joint segmentation of optic disc and optic cup for glaucoma screening," *IEEE Access*, vol. 8, pp. 102733–10274, 2020.

[19] M. M. R. Krishnan and O. Faust, "Automated glaucoma detection using hybrid feature extraction in retinal fundus images," *Journal of Mechanics in Medicine and Biology*, vol. 13(1), pp. 1350011–1350032, 2013.

[20] Q. Abbas. "Glaucoma-deep: detection of glaucoma eye disease on retinal fundus images using deep learning," *International Journal of Advanced Computer Science and Applications*, vol. 8(6), pp. 41–45, 2017.

[21] H. Ahmad, A. Yamin, A. Shakeel, S. O. Gillani and U. Ansari, "Detection of glaucoma using retinal fundus images," In *Proceedings of International Conference on Robotics and Emerging Allied Technologies in Engineering (iCREATE)*, IEEE, 2014, pp. 321–324.

[22] A. C. Thompson, A. A. Jammal, S. I. Berchuck, E. B. Mariottoni and F.A. Medeiros, "Assessment of a segmentation-free deep learning algorithm for diagnosing glaucoma from optical coherence tomography scans," *JAMA Ophthalmology*, vol. 138(4), pp. 333–339, 2020.

[23] W. Liao, B. Zou, R. Zhao, Y. Chen, Z. He and M. Zhou, "Clinical interpretable deep learning model for glaucoma diagnosis," *IEEE Journal of Biomedical and Health Informatics*, vol. 24(5), pp. 1405–1412, 2019.

[24] J. Camara, A. Neto, I. M. Pires, M. V. Villasana, E. Zdravevski and A. Cunha, "Literature review on artificial intelligence methods for glaucoma screening, segmentation, and classification," *Journal of Imaging*, vol. 8(2), p. 1–28, 2022.

[25] A. O. Joshua, F. V. Nelwamondo and G. Mabuza-Hocquet, "Segmentation of optic cup and disc for diagnosis of glaucoma on retinal fundus images," In *Proceedings of Southern African Universities Power Engineering Conference/Robotics and Mechatronics/Pattern Recognition Association of South Africa (SAUPEC/RobMech/PRASA)*, IEEE, 2019, pp. 183–187.

[26] F. Khan, S. A. Khan, U. U. Yasin, I. ul Haq and U. Qamar, "Detection of glaucoma using retinal fundus images," In *Proceedings of 6th Biomedical Engineering International Conference,* IEEE, 2013, pp. 1–5, 2013.

[27] M. R. K. Mookiah, U. R. Acharya, C. K. Chua, L. C. Min, E. Y. K. Ng, M. M. Mushrif and A. Laude, "Automated detection of optic disk in retinal fundus images using intuitionistic fuzzy histon segmentation," In *Proceedings of the Institution of Mechanical Engineers, Part H: Journal of Engineering in Medicine*, 2013, vol. 227(1), pp. 37–49.

[28] I. Qureshi, "Glaucoma detection in retinal images using image processing techniques: a survey," *International Journal of Advanced Networking and Applications*, vol. 7(2), p. 2705–2718, 2015.

[29] M. N. Bajwa, M. I. Malik, S. A. Siddiqui, A. Dengel, F. Shafait, W. Neumeier and S. Ahmed, "Two-stage framework for optic disc localization and glaucoma classification in retinal fundus images using deep learning," *BMC Medical Informatics and Decision Making*, vol. 19(1), pp. 1–16, 2019.

[30] G. Du, X. Cao, J. Liang, X. Chen and Y. Zhan, "Medical Image Segmentation based on U-Net: A Review," *Journal of Imaging Science & Technology*, vol. 64(2), pp. 020508-1–020508-12, 2020.

[31] M. Tan and Q. Le, "Efficientnet: Rethinking model scaling for convolutional neural networks," In *Proceedings of International Conference on Machine Learning*, PMLR, 2019, pp. 6105–6114.

[32] F. Guo, W. Li, J. Tang, B. Zou and Z. Fan, "Automated glaucoma screening method based on image segmentation and feature extraction," *Medical & Biological Engineering & Computing*, vol. 58, pp. 2567–2586, 2020.

[33] R. Krishnan, V. Sekhar, J. Sidharth, S. Gautham and G. Gopakumar, "Glaucoma detection from retinal fundus images," In *Proceedings of 2020 International Conference on Communication and Signal Processing (ICCSP)*, IEEE, 2020, pp. 0628–0631.